In Situ Formation of Cobalt Oxide Nanocubanes as Efficient Oxygen Evolution Catalysts

Gregory S. Hutchings,[†,§] Yan Zhang,[†,§] Jian Li,[‡] Bryan T. Yonemoto,[†] Xinggui Zhou,[‡] Kake Zhu,*[,‡] and Feng Jiao*[,†]

[†]Center for Catalytic Science & Technology (CCST), Department of Chemical and Biomolecular Engineering, University of Delaware, Newark, Delaware 19716, United States

[‡]UNILAB, State Key Lab of Chemical Engineering, School of Chemical Engineering, East China University of Science and Technology, 130 Meilong Road, Shanghai 200237, P. R. China

S *Supporting Information*

ABSTRACT: Oxygen evolution from water poses a significant challenge in solar fuel production because it requires an efficient catalyst to bridge the one-electron photon capture process with the four-electron oxygen evolution reaction (OER). Here, a new strategy was developed to synthesize nonsupported ultrasmall cobalt oxide nanocubanes through an *in situ* phase transformation mechanism using a layered $Co(OH)(OCH_3)$ precursor. Under sonication, the precursor was exfoliated and transformed into cobalt oxide nanocubanes in the presence of $NaHCO_3$–Na_2SiF_6 buffer solution. The resulting cobalt catalyst with an average particle size less than 2 nm exhibited a turnover frequency of 0.023 per second per cobalt in photocatalytic water oxidation. X-ray absorption results suggested a unique nanocubane structure, where 13 cobalt atoms fully coordinated with oxygen in an octahedral arrangement to form 8 Co_4O_4 cubanes, which may be responsible for the exceptionally high OER activity.
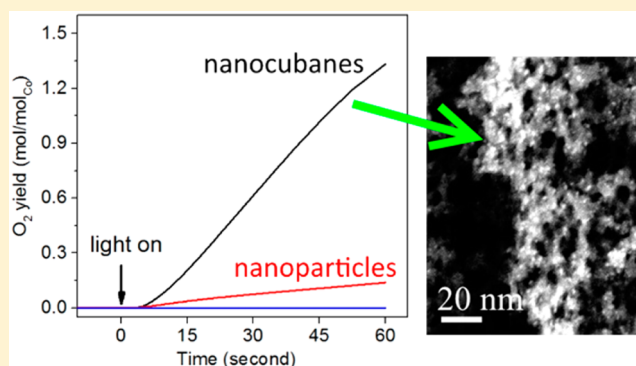
INTRODUCTION

A sustainable energy future heavily depends on the capability to store energy in a cheap and efficient way, because of the mismatch between energy demand and intermittent power generation from renewable energy sources (e.g., solar panels, biomass, wind, and wave energy). Liquid fuel is an ideal medium for energy storage, because it can easily be stored and used in the current energy infrastructure.[1,2] In the past decades, many approaches have been proposed and investigated for fuel production from water and carbon dioxide through artificial photosynthesis.[3−7] Regardless of which approach is used, catalytic oxygen evolution from water is the critical half reaction, because it provides electrons and protons for solar fuel production through either hydrogen evolution or proton-assisted CO_2 reduction to hydrocarbons.[8−20] For solar fuel production on a terawatt scale, visible-light driven water oxidation is the only way that we can potentially produce sufficient protons and electrons economically. However, photocatalytic oxygen evolution reaction (OER) has slow kinetics and requires large overpotentials, because oxygen evolution from water is a four-electron reaction, while photon capture is a single electron/hole process.[3] Therefore, a multielectron catalyst is essential for efficient visible-light-driven water oxidation.

Cobalt-based OER catalysts, especially Co_3O_4 spinel, have been intensively studied in photocatalytic systems because of their superior properties, good stability, and high abundance.[4−6,21−26] There are two distinct cobalt sites in Co_3O_4 spinel: four-oxygen coordinated tetrahedral sites and six-oxygen coordinated octahedral sites. The octahedral cobalt atoms and neighboring oxygen atoms are in a Co_4O_4 cubane arrangement, which has been suggested to be crucial for OER.[27] In our previous work, we have synthesized a series of metal-doped Co_3O_4 nanoparticles and mesopores and investigated their OER activity under visible light at near-neutral pH conditions.[28,29] The results agree well with the speculation that the OER active site in spinel is the octahedral Co^{3+}. Therefore, in an ideal OER catalyst cobalt atoms have an average oxidation state of 3+ and form Co_4O_4 cubanes. An extremely small particle size is desired to ensure that most of cobalt atoms sitting on the particle surface act as catalytic centers for oxygen evolution, but at the same time the particles must remain stable (ideally under near-neutral pH conditions). It is also important for the catalyst to be freestanding without any inert support so that it can be directly attached to semiconductors. However, there are only very few catalysts that meet all the requirements.

In a traditional solution synthesis, nanoparticles aggregate easily during drying and redispersing processes, especially those surfactant-free or support-free particles. Here, we report a new strategy to synthesize freestanding, ultrasmall, and highly active cobalt oxide nanocubanes with an average cobalt oxidation state close to 3+ through an *in situ* phase transformation mechanism. The new approach enables us to prepare freestanding ultrasmall nanoparticles directly inside the reaction solution without the presence of any surfactant or inert support. A new layered cobalt compound, $Co(OH)(OCH_3)$, was first synthesized as the precursor of the cobalt oxide nanocubane catalyst using a solvothermal method. The precursor, upon sonication, was exfoliated and transformed into cobalt oxide clusters in the reaction buffer. X-ray absorption spectra for the postreaction catalyst show that the cobalt catalyst under reaction conditions contains multiple Co_4O_4 cubanes with an average cobalt oxidation state of ~2.8+. An exceptional turnover frequency (TOF) of 0.023 per second per cobalt atom was observed for the cobalt oxide nanocubanes, which represents the highest TOF reported to date for nonprecious metal based OER catalysts driven by visible light.

■ RESULTS

Synthesis and Characterization of Cobalt Catalyst. The layered $Co(OH)(OCH_3)$ was obtained by treating a cobalt(II) acetate tetrahydrate methanol solution in a sealed hydrothermal bomb at 180 °C. A typical scanning electron microscopy (SEM) image of the as-synthesized $Co(OH)$-(OCH_3) is shown in Figure 1a, in which a nanoflake-like morphology is evident. The typical size of each flake is approximately 0.5−2 μm in diameter and 20−50 nm in
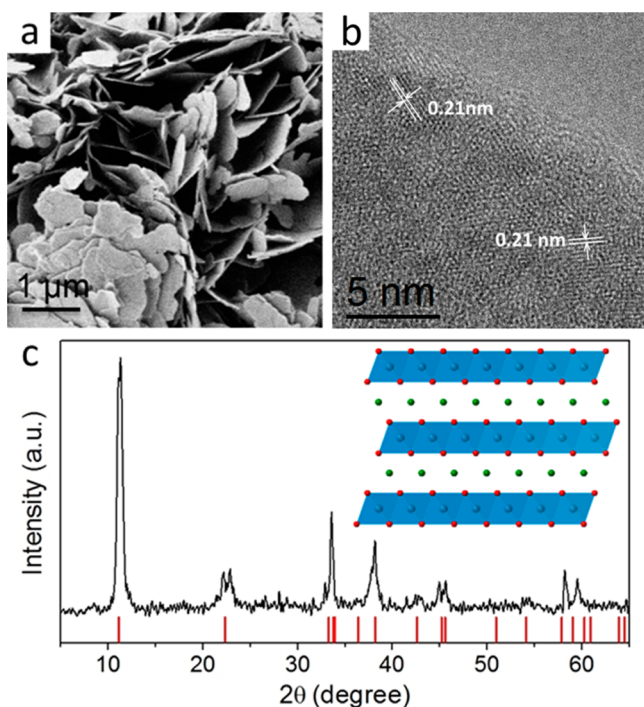

Figure 1. (a) A typical SEM image, (b) HRTEM image, and (c) PXRD pattern for as-synthesized layered $Co(OH)(OCH_3)$ compound. The red bars in (c) represent the expected diffraction peaks for the simulated structure. The inset in (c) is the model structure of the layered $Co(OH)(OCH_3)$ compound. Blue ball, Co; red ball, O; green ball, H or CH_3.

thickness. A close examination of the as-made flake using high-resolution transmission electron microscopy (HRTEM) revealed its polycrystalline nature (Figure 1b). To identify the crystal structure of $Co(OH)(OCH_3)$, the as-made cobalt compound was examined using powder X-ray diffraction (PXRD) and a few diffraction peaks were clearly observed (Figure 1c). However, the PXRD pattern does not match any existing compound in the Inorganic Crystal Structure Database (ICSD), indicating that it may be an unknown crystal structure. Because of its highly polycrystalline nature, it is not possible to solve the crystal structure of $Co(OH)(OCH_3)$ using single crystal X-ray diffraction. Previous work on $Ni(OH)(OCH_3)$ and $Ni_xMg_{1-x}(OH)(OCH_3)$ (0 < x < 1) reported a very similar layered structure, which provides us an opportunity to use it as a model structure for the cobalt compound.[30,31] Here, we used the General Structure Analysis System (GSAS) software to create a model of $Co(OH)(OCH_3)$ based on the crystal structures of $Ni_xMg_{1-x}(OH)(OCH_3)$ and $LiCoO_2$ with a space group of $R\bar{3}m$ (more details in Supporting Information Table S1). Interlayer atoms were excluded from the simulation due to their highly disordered nature. As can be seen in Figure 1c, the simulated PXRD pattern (red bars in Figure 1c) matches that of as-made cobalt precursor very well, indicating that the simulated structure is likely to be the actual crystal structure for the cobalt precursor (a model structure shown in Figure 1c, inset). There is one additional peak at ~23° which does not directly match the simulated PXRD pattern for $Co(OH)$-(OCH_3). This could be due to the scattering of interlayer atoms or a small amount of unknown impurity. The composition of $Co(OH)(OCH_3)$ was also confirmed by thermogravimetric analysis (Supporting Information Figure S1). A 25% weight loss was observed when the sample was heated in air to 600 °C. This observed loss is consistent with the expected value of the conversion of $Co(OH)(OCH_3)$ to Co_3O_4 through thermal decomposition. The structure of $Co(OH)(OCH_3)$ was further examined by Fourier transform infrared spectroscopy (FTIR). The FTIR spectrum is almost identical to that of $Ni_xMg_{1-x}(OH)(OCH_3)$, indicating that they may share a similar structure. (Supporting Information Figure S2).[31,32] *In situ* transformation of the layered $Co(OH)(OCH_3)$ precursor to the free-standing cobalt oxide nanocubane catalyst was performed using a simple sonication treatment in the presence of $NaHCO_3$−Na_2SiF_6 buffer (pH = 5.8). It should be noted that $Co(OH)(OCH_3)$ precursor (Figure 2a) is not soluble in $NaHCO_3$−Na_2SiF_6 buffer under magnetic stirring, while a transparent pink solution can be formed using ultrasonication (Figure 2a). Once it is transparent, the solution was stable for days and no precipitation could be observed.

To determine the structure of *in situ* formed cobalt catalyst, we first examined its morphology using electron microscopy analysis. The SEM image in Figure 2b clearly shows that upon sonication nanoflake like morphology disappeared and very small clusters were formed. The large structures in the SEM image correspond to dried components of the buffer solution. To elucidate the formation mechanism of the cobalt oxide nanocubanes, we performed a control experiment, in which layered $Co(OH)(OCH_3)$ precursor was sonicated in water instead of a $NaHCO_3$−Na_2SiF_6 buffer solution. No nanocubanes can be observed and the nanoflake morphology of precursor was preserved (Supporting Information Figure S3a). Further examination of cobalt catalyst was performed in STEM. Extremely small clusters were clearly observed for the sample sonicated in buffer, visible as bright dots on the dried buffer
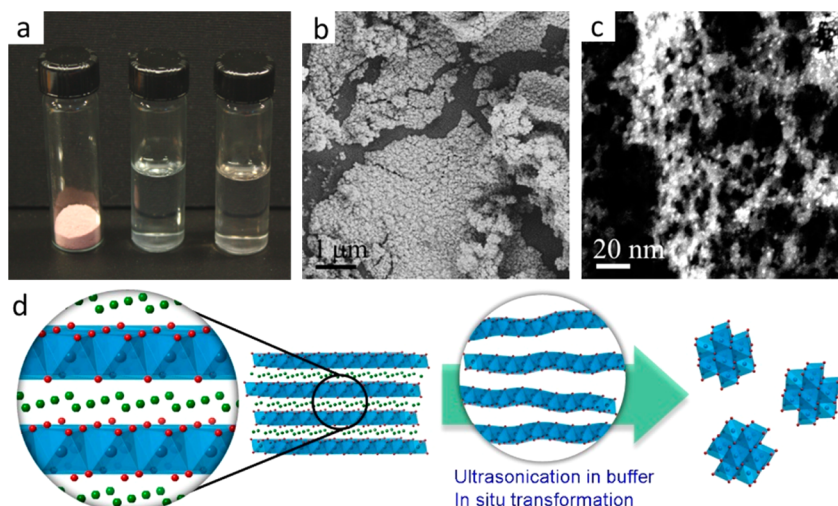
Figure 2. (a) Photographs of the $Co(OH)(OCH_3)$ precursor, buffer solution, and *in situ* formed cobalt oxide nanocubanes in buffer, from left to right. (b) SEM and (c) STEM images for layered $Co(OH)(OCH_3)$ after sonication in buffer. The large structures in (b) and (c) are precipitates from buffer components. (d) Schematic of the formation of cobalt oxide nanocubanes via sonication of the $Co(OH)(OCH_3)$ precursor in the buffer solution.

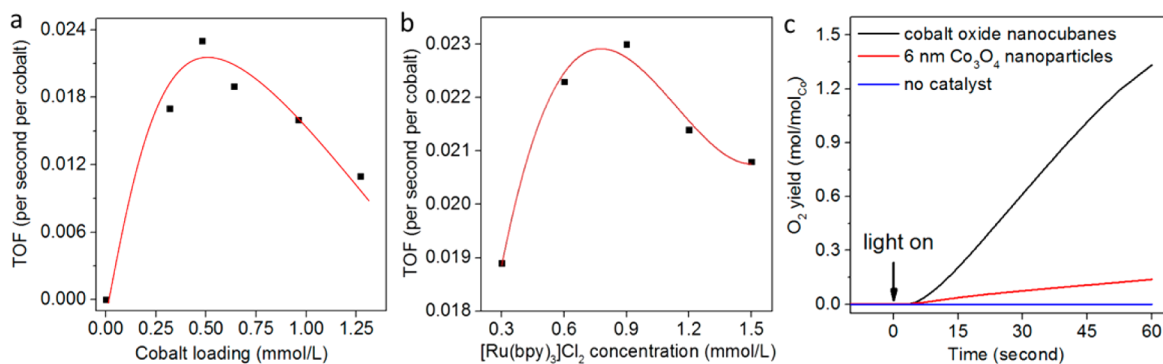**Figure 3.** (a) Cobalt oxide nanocubane catalyst loadings vs TOFs with a $[Ru(bpy)_3]Cl_2$ concentration of 0.9 mmol/L. (b) $[Ru(bpy)_3]Cl_2$ concentrations vs TOFs with a cobalt oxide nanocubane catalyst loading of 0.48 mmol/L. The red lines in (a) and (b) indicate the trends of TOF change. (c) Oxygen evolution activities for cobalt oxide nanocubanes (black curve) and 6 nm Co_3O_4 nanoparticles (red curve). Experiment without the presence of catalyst showed no oxygen generation (blue curve).

salts (Figure 2c). The particle size distribution (Supporting Information Figure S4) clearly confirms that the average size of cobalt oxide nanocubanes is below 2 nm. However, the sample treated in deionized water did not show any significant change in morphology (Supporting Information Figure S3b). In another control experiment, we sonicated the precursor in a diluted HCl solution (pH = 5.8), which resulted in a partial transformation of layered cobalt precursor to small clusters with a broad size distribution. Both control experiments suggest that a slightly acidic environment and the buffer itself played some critical roles in the formation of cobalt oxide nanocubanes. The overall *in situ* transformation process is summarized in Figure 2d for the cobalt oxide nanocubane formation. Identification of the atomic structure of *in situ* formed cobalt oxide clusters will be discussed later together with X-ray absorption results.

Catalyst Evaluation. Photocatalytic oxygen evolution from water was performed using a well-established $[Ru(bpy)_3]^{2+}$-$S_2O_8^{2-}$ (bpy = bipyridyl) system in an aqueous $NaHCO_3$–Na_2SiF_6 buffer (pH = 5.8). The details of the $[Ru(bpy)_3]^{2+}$-$S_2O_8^{2-}$ photocatalytic cycle can be found in our previous publications or other literature.[28,33,34] In a typical reaction, a mixture containing a certain amount of cobalt catalyst, persulfate, sensitizer, and 2.2 mL of buffer was placed in a

Clark electrode reactor. After bubbling with helium gas for 5–10 min, the reactor was exposed to a 300 Xe lamp equipped with a 400 nm cutoff filter and the oxygen concentration in the solution was recorded. To obtain the optimal result, we first varied the cobalt catalyst loading and investigated catalyst loading effects. A maximum TOF of 0.023 s^{-1} Co^{-1} was observed at a cobalt loading of approximately 0.5 mmol/L (Figure 3a). Then, we fixed the cobalt catalyst loading at 0.48 mmol/L and investigated how $[Ru(bpy)_3]^{2+}$ sensitizer concentration affects the TOF of oxygen evolution from water. On the basis of the results shown in Figure 3b, the activity dependence on sensitizer concentration is weak as long as a minimum amount of sensitizer is present in the system. The optimal sensitizer concentration is around 0.9 mmol/L. To demonstrate the superior catalytic properties of *in situ* formed cobalt oxide nanocubanes, we also synthesized Co_3O_4 nanoparticles with an average particle size of 6 nm using a prior reported hydrothermal route.[26] The 6 nm Co_3O_4 nanoparticles were tested at the identical conditions (cobalt loading of 0.48 mmol/L and sensitizer concentration of 0.9 mmol/L). The results (Figure 3c) clearly show that the TOF of *in situ* formed cobalt oxide nanocubanes (~0.023 s^{-1} Co^{-1}) is more than ten times higher than that of 6 nm Co_3O_4 nanoparticles (~0.002 s^{-1}
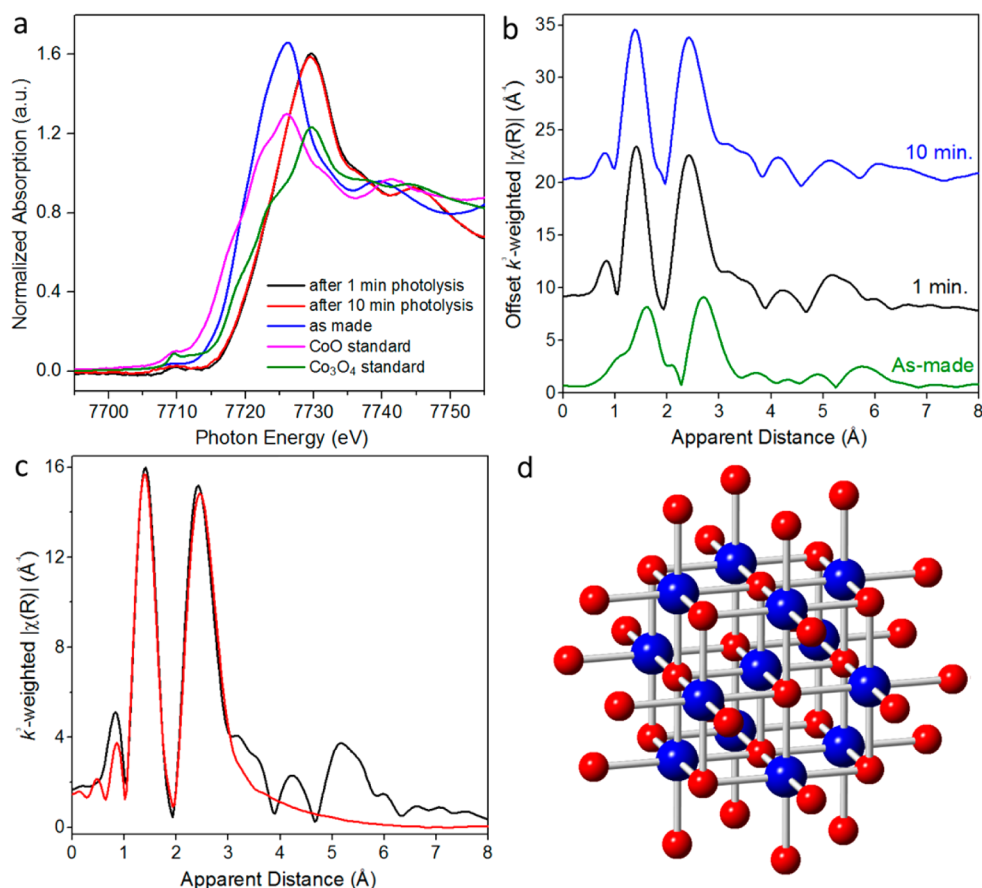
Figure 4. (a) K-edge XANES spectra of as-made Co(OH)(OCH$_3$) compound (blue line), the catalyst after 1 min reaction (black line), the catalyst after 10 min reaction (red line) and two standards: CoO (magenta line) and Co$_3$O$_4$ (green line). (b) EXAFS spectra for the as-made (green line), postreaction after 1 min (black line), and postreaction after 10 min (blue line) samples, and (c) result of fitting the first Co−O and Co−Co single-scattering paths (red line). The proposed structure of the cobalt oxide nanocubane material generated *in situ* is shown in (d). The blue and red spheres represent cobalt and oxygen atoms, respectively.

Co^{-1}), one of the state-of-the-art cobalt-based spinel catalysts. For comparison, we have reviewed recent literature of cobalt-based OER catalysts driven by visible light (Supporting Information Table S2). The TOF of cobalt oxide nanocubane is the highest value reported to date among all the nonprecious metal based water oxidation catalysts driven by visible light. Regarding catalyst stability, the current setup (i.e., Clark electrode and [Ru(bpy)$_3$]$^{2+}$ sensitizer) is not an ideal system to study photocatalytic activity over a long period of time. Follow-up work will be performed in a more robust semiconductor based system.

Atomic Structure of Cobalt Catalyst. To elucidate the origin of the exceptional OER activity for *in situ* formed cobalt catalyst, it is crucial to identify its atomic structure. We first attempted to separate the catalyst particles from the solution. However, the nanocubanes are too small to be separated via a traditional centrifuge method, making it not possible to perform bulk structural characterizations, such as PXRD and gas absorption. Therefore, we employed X-ray absorption spectroscopy (XAS), a very useful tool to probe the structure of small clusters,[35] to extract structural information on the cobalt oxidation state and coordination environment for *in situ* formed catalyst. The X-ray absorption near-edge structure (XANES) data for the Co K-edge in Figure 4 show a clear edge shift to high energy for the layered Co(OH)(OCH$_3$) after 1 min of photolysis, while no further edge shift in the spectrum was

observed between the 1 and 10 min postreaction data (Figure 4a), indicating that the phase transformation from layered precursor to cobalt oxide nanocubane was finished after sonication in the buffer solution and within 1 min of visible light radiation. On the basis of the edge positions of catalysts and standards (Figure 4a), the estimated average oxidation states of cobalt precursor and *in situ* formed catalyst are +2.2 and +2.8, respectively. The oxidation of Co^{2+} in the precursor to a higher oxidation state is very likely due to the highly oxidizing environment for photocatalytic oxygen evolution.

The atomic structure of cobalt oxide nanocubanes was further investigated using extended X-ray absorption fine structure (EXAFS). The as-made layered precursor showed two well-defined peaks in R-space at 1.7 and 2.9 Å (all the distances discussed here are apparent distances without phase correction), corresponding to the cobalt−oxygen and cobalt−cobalt distances in the cobalt oxide layer (Figure 4b). Because of the polycrystalline nature of the layered compound, no distinguishable peaks at long distances are observed. To explore the atomic structure of catalyst in working conditions, we run the photocatalytic OER reaction in a large batch type reactor for more than 10 min. The EXAFS data for both 1 and 10 min postreaction catalysts show almost identical characteristics in R-space, with one major peak at 1.4 Å and the other at 2.4 Å, suggesting that the cobalt nanocubanes were formed within the first minute of reaction. The postreaction data also suggest a

good stability of the *in situ* formed nanocubanes. The contraction of Co—O and Co—Co bond distances is also consistent with the observed oxidation state increase that occurs during reaction.

DISCUSSION

Spinel-type cobalt oxides have been investigated as potential OER catalysts in both photochemical and electrochemical systems. In a typical Co_3O_4 spinel structure, octahedral cobalt atoms and neighbor oxygen atoms form Co_4O_4 cubanes, which are likely the activity sites for oxygen evolution in a manner similar to the Mn_4CaO_5 catalytic site in nature's photosystem II.[36] Therefore, it is important to check whether *in situ* formed cobalt catalyst contains Co_4O_4 cubanes in its structure. Curve-fitting was performed for the EXAFS spectrum of the 1 min postreaction sample. The results are shown in Figure 4c and the fitting details can be found in Supporting Information Table S3 and Figure S5. Assuming that Co atoms are fully coordinated by O atoms with an octahedral arrangement, the Co—O coordination number was fixed at 6 during the fitting. All other parameters were allowed to vary within physically meaningful ranges. By considering the first Co—O and Co—Co single-scattering paths, we found a Co—Co coordination of 5.8 ± 0.6. On the basis of the fitting, we propose a nanocubane structure consisting of 13 cobalt atoms per cluster with a particle size of ~1.1 nm (Figure 4d). Although we did not include any hydrogen atoms in the model, it is possible that some of the outer layer oxygen atoms are actually hydroxide groups. The proposed nanocubane structure has a Co—Co coordination of 5.5, which is in agreement of the fitting result. Expanded analysis of the next two features in *R*-space indicate that they represent additional Co—O and Co—Co scattering at distances consistent with the cluster of cobalt octahedra. The additional peaks with low intensities may also result from long-range ordering of some large clusters. It should be noted that distinct from previous work on phosphate-derived Co-Pi catalysts and Co_3O_4 spinels, the proposed structure contains a large number of Co_4O_4 cubanes in a small cluster (8 Co_4O_4 with 13 Co atoms).[37,38] It is very likely that the unique biomimetic Co_4O_4 cubanes are responsible for the exceptional photocatalytic water oxidation activity of cobalt oxide nanocubanes.

In a recent mechanistic study, water oxidation intermediates have been observed using time-resolved FTIR technique.[39] Frei and his co-workers studied the behavior of Co_3O_4 nanoparticles in the visible light driven $[Ru(bpy)_3]^{2+}$-$S_2O_8^{2-}$ system. They proposed two distinct active sites, namely oxo-bridged Co(III)OH binuclear site and single Co(III)OH sites. The time-resolved FTIR results suggested that the presence of adjacent CoOH groups coupled with an oxygen bridge could lead to a fast reactive site with a TOF higher than 3 s^{-1}, while the single cobalt site exhibited a much slower TOF (~0.02 s^{-1} per surface atom). In our cobalt oxide nanocubane catalyst, 12 out of 13 cobalt atoms are on the surface and all the cobalt octahedra are interconnected with edge sharing, which, based on Frei's mechanism, should result in a much higher turnover than what was observed in our experiments (0.023 s^{-1} Co^{-1}). It should be noted that the TOF observed for cobalt oxide nanocubanes is at the same order of magnitude of that observed for single site Co catalyst reported by Tilley and his co-workers (~0.014 s^{-1} Co^{-1}).[40] Therefore, we suspect that regardless of the presence of a second Co(III)OH at the adjacent site, the dominant reaction pathway for cobalt oxide catalyst may be the single Co(III)OH site mechanism. There are several potential

reasons why a significantly higher TOF has not been observed yet. For instance, hole injection from $[Ru(bpy)_3]^{2+}$ sensitizer to the adjacent Co(III)OH site could be difficult considering the large size of $[Ru(bpy)_3]^{2+}$ complex (~11 Å) compared to the Co—O—Co distance (~2.8 Å). Additionally, charge transfer from the sensitizer to the active site is a random process with no control of directionality, which also reduces the chance for the two neighboring cobalt atoms to be cooperative. A precise control of charge transfer may be required to achieve a higher TOF. Further investigation will be required to fully determine the oxygen evolving reaction mechanism on the surface of cobalt oxide nanocubanes.

CONCLUSION

In summary, we have successfully synthesized cobalt oxide nanocubanes with a particle size less than 2 nm through an *in situ* transformation process under a photocatalytic environment. Each *in situ* formed nanocubane contains 13 cobalt atoms, fully coordinated with oxygen atoms to form 8 Co_4O_4 cubanes. The nanocubanes exhibited an order of magnitude higher TOF in photocatalytic water oxidation activity compared to traditional 6 nm Co_3O_4 spinel nanoparticles. The performance of the nanocubane catalyst represents the highest TOF that has been reported to date among all nonprecious metal oxide OER catalysts. The *in situ* formed cobalt nanocubanes are free-standing and support-free, which may be implemented in a wide range of photocatalytic systems.

METHODS

Material Synthesis. The synthetic procedure of $Co(OH)(OCH_3)$ was modified from a previous report of $Mg(OH)(OCH_3)$.[41] In a typical synthesis, 0.01 mol of cobalt acetate tetrahydrate was dissolved in 100 mL of anhydrous methanol. The solution was then transferred into a hydrothermal bomb (200 mL) and placed in an oven at 180 °C for 24 h. After the solvothermal treatment, the bomb was cooled down to room temperature. The sample was recovered by filtering, washed with dry methanol, and dried in air.

The synthesis of 6 nm Co_3O_4 spinel nanoparticles was reported in our previous study of metal-doped Co_3O_4 spinel nanoparticles.[29] In a typical procedure, 0.50 g of $Co(CH_3COO)_2 \cdot 4H_2O$ (2 mmol) was mixed with 2 mL water and 23 mL ethanol in a 40 mL Teflon liner. Then, a 2.5 mL of aqueous ammonia solution (wt. 25%) was added under stirring. After stirring for 10 min, a brownish-gray slurry was formed and the liner containing the suspension was carefully sealed in an autoclave, which was treated at 150 °C for 3 h. After the autoclave was cooled down to room temperature in air, the product was collected by washing with deionized water, following by a drying process at 60 °C.

Structural Characterizations. Powder X-ray diffraction (PXRD) measurements were performed using a PANalytical X'Pert X-ray diffractometer using Cu Kα radiation. FTIR spectrum was collected using a Nicolet Nexus 470 FTIR instrument equipped with an MCT-A detector. Scanning electron microscopy (SEM) images were collected using a Zeiss Auriga-60. Transmission and scanning transmission electron microscopy (TEM and STEM) imaging were conducted on a JEOL JEM-2010F equipped with a high angle annular dark field (HAADF) detector and operated at 200 kV.

Photocatalytic Activity Test. The detailed procedure of photocatalytic oxygen evolution from water has been reported in our previous publication.[29] In this work, a few modifications have been made. In a typical preparation of cobalt oxide nanocubane catalyst, cobalt precursor was dispersed in aqueous Na_2SiF_6—$NaHCO_3$ buffer with a pH value of 5.8 by sonication for 20 min prior to photolysis. In a typical experiment, a certain amount of catalyst and $Ru(bpy)_3Cl_2 \cdot 6H_2O$, 7.1 mg of $Na_2S_2O_8$, and 21.5 mg of Na_2SO_4 were mixed in 2.2 mL of buffer, followed by purging with helium gas until oxygen

concentration reached its minimum (recorded as the baseline). Then, the Clark electrode system was exposed to a 300 W Xe research lamp (UV fused silica, 1.3 in collimated, $F/1$, 1.5 in.) with a 400 nm cutoff filter. During exposure to light, the oxygen concentration was monitored for at least 1 min. Additionally, control experiments were also performed to ensure that the photocatalytic water oxidation driven by the cobalt catalysts is the oxygen source. Experiments without either catalyst or $Ru(bpy)_3Cl_2$ sensitizer gave no oxygen production.

XAS Measurement and Analysis. The samples were mixed with amorphous SiO_2 powder and sealed in polyimide tape for the XAS measurements. We also collected XAS data for bulk CoO and Co_3O_4 standards under identical conditions for comparison. Co K-edge XAS spectra were recorded on beamline X18A of the National Synchrotron Light Source at Brookhaven National Laboratory. A Si(111) channel cut monochromator was employed to sweep the incident X-ray energy through the measurement range, and a rhodium-coated focusing mirror was used to direct the beam into the measurement hutch. The beamline resolution is approximately $5 \times 10^{-4} \Delta E/E$. Since the postreaction materials were necessarily prepared with relatively low concentration, data collection was optimized for fluorescence with a PIPS detector. The free Demeter software package was used for all data alignment, reduction, and postprocessing (Athena), as well as EXAFS fitting analysis (Artemis).[42] Energy measurements were calibrated to the known edge position of a pure Co foil (7709 eV).

Simulated scattering paths were fit to the data via the EXAFS equation:

$$\chi(k) = S_0^2 \sum_j \frac{N_j e^{-2k^2\sigma_j^2} e^{-(2R_j/\lambda(k))} f_j(k)}{kR_j^2} \sin[2kR_j + \delta_j(k)]$$

where k is the wavenumber of the photoelectron, S_0^2 is the amplitude reduction factor, N_j is the coordination number for a particular path, σ^2 is the mean square displacement factor (disorder), R_j is the path length, $\lambda(k)$ is the mean free path of the photoelectron, $f_j(k)$ is the scattering amplitude function, and $\delta_j(k)$ is the phase shift. For the fitting results represented in Figure 4c and Supporting Information Table S3, the following variables were parametrized and optimized: N_j and S_0^2 (inverse relationship), R_j, σ^2, and the energy deviation between theory and experiment, ΔE_0.

ASSOCIATED CONTENT

Ⓢ Supporting Information

Crystal structure simulation information, thermogravimetric results, FTIR spectrum for the as-made cobalt compound, additional SEM and STEM images, TOFs for cobalt-based catalysts, and EXAFS fitting parameters. This material is available free of charge via the Internet at http://pubs.acs.org.

AUTHOR INFORMATION

Corresponding Authors
*jiao@udel.edu
*kakezhu@ecust.edu.cn

Author Contributions
§These authors contributed equally.

Notes
The authors declare no competing financial interest.

ACKNOWLEDGMENTS

REFERENCES

(1) Scholes, G. D.; Fleming, G. R.; Olaya-Castro, A.; van Grondelle, R. *Nat. Chem.* **2011**, *3*, 763−774.
(2) Dahl, S.; Chorkendorff, I. *Nat. Mater.* **2012**, *11*, 100−101.
(3) Hurst, J. K. *Science* **2010**, *328*, 315−316.
(4) Jiao, F.; Frei, H. *Energy Environ. Sci.* **2010**, *3*, 1018−1027.
(5) Kanan, M. W.; Nocera, D. G. *Science* **2008**, *321*, 1072−1075.
(6) Rosen, J.; Hutchings, G. S.; Jiao, F. *J. Am. Chem. Soc.* **2013**, *135*, 4516−4521.
(7) Lu, Q.; Rosen, J.; Zhou, Y.; Hutchings, G. S.; Kimmel, Y. C.; Chen, J. G. G.; Jiao, F. *Nat. Commun.* **2014**, *5*, 3242.
(8) Blakemore, J. D.; Schley, N. D.; Balcells, D.; Hull, J. F.; Olack, G. W.; Incarvito, C. D.; Eisenstein, O.; Brudvig, G. W.; Crabtree, R. H. *J. Am. Chem. Soc.* **2010**, *132*, 16017−16029.
(9) Concepcion, J. J.; Tsai, M. K.; Muckerman, J. T.; Meyer, T. J. *J. Am. Chem. Soc.* **2010**, *132*, 1545−1557.
(10) Gorlin, Y.; Jaramillo, T. F. *J. Am. Chem. Soc.* **2010**, *132*, 13612−13614.
(11) Yin, Q. S.; Tan, J. M.; Besson, C.; Geletii, Y. V.; Musaev, D. G.; Kuznetsov, A. E.; Luo, Z.; Hardcastle, K. I.; Hill, C. L. *Science* **2010**, *328*, 342−345.
(12) Zhong, D. K.; Gamelin, D. R. *J. Am. Chem. Soc.* **2010**, *132*, 4202−4207.
(13) Berardi, S.; La Ganga, G.; Natali, M.; Bazzan, I.; Puntoriero, F.; Sartorel, A.; Scandola, F.; Campagna, S.; Bonchio, M. *J. Am. Chem. Soc.* **2012**, *134*, 11104−11107.
(14) Han, X. B.; Zhang, Z. M.; Zhang, T.; Li, Y. G.; Lin, W. B.; You, W. S.; Su, Z. M.; Wang, E. B. *J. Am. Chem. Soc.* **2014**, *136*, 5359−5366.
(15) Hong, D. C.; Yamada, Y.; Nagatomi, T.; Takai, Y.; Fukuzumi, S. *J. Am. Chem. Soc.* **2012**, *134*, 19572−19575.
(16) Zidki, T.; Zhang, L. H.; Shafirovich, V.; Lymar, S. V. *J. Am. Chem. Soc.* **2012**, *134*, 14275−14278.
(17) Bajdich, M.; Garcia-Mota, M.; Vojvodic, A.; Norskov, J. K.; Bell, A. T. *J. Am. Chem. Soc.* **2013**, *135*, 13521−13530.
(18) Lu, Z. Y.; Wang, H. T.; Kong, D. S.; Yan, K.; Hsu, P. C.; Zheng, G. Y.; Yao, H. B.; Liang, Z.; Sun, X. M.; Cui, Y. *Nat. Commun.* **2014**, *5*, 4345.
(19) Song, F.; Hu, X. L. *Nat. Commun.* **2014**, *5*, 4477.
(20) Wang, W. Y.; Chen, J.; Li, C.; Tian, W. M. *Nat. Commun.* **2014**, *5*, 4647.
(21) Grewe, T.; Deng, X. H.; Weidenthaler, C.; Schuth, F.; Tuysuz, H. *Chem. Mater.* **2013**, *25*, 4926−4935.
(22) Del Pilar-Albaladejo, J.; Dutta, P. K. *ACS Catal.* **2014**, *4*, 9−15.
(23) Lv, H. J.; Song, J.; Geletii, Y. V.; Vickers, J. W.; Sumliner, J. M.; Musaev, D. G.; Kogerler, P.; Zhuk, P. F.; Bacsa, J.; Zhu, G. B.; Hill, C. L. *J. Am. Chem. Soc.* **2014**, *136*, 9268−9271.
(24) Sun, K.; Shen, S. H.; Liang, Y. Q.; Burrows, P. E.; Mao, S. S.; Wang, D. L. *Chem. Rev.* **2014**, *114*, 8662−8719.
(25) Grzelczak, M.; Zhang, J. S.; Pfrommer, J.; Hartmann, J.; Driess, M.; Antonietti, M.; Wang, X. C. *ACS Catal.* **2013**, *3*, 383−388.
(26) Liao, M. J.; Feng, J. Y.; Luo, W. J.; Wang, Z. Q.; Zhang, J. Y.; Li, Z. S.; Yu, T.; Zou, Z. G. *Adv. Funct. Mater.* **2012**, *22*, 3066−3074.
(27) Gardner, G. P.; Go, Y. B.; Robinson, D. M.; Smith, P. F.; Hadermann, J.; Abakumov, A.; Greenblatt, M.; Dismukes, G. C. *Angew. Chem., Int. Ed.* **2012**, *51*, 1616−1619.
(28) Yusuf, S.; Jiao, F. *ACS Catal.* **2012**, *2*, 2753−2760.
(29) Zhang, Y.; Rosen, J.; Hutchings, G. S.; Jiao, F. *Catal. Today* **2014**, *225*, 171−176.
(30) Lebihan, S.; Guenot, J.; Figlarz, M. *J. Solid State Chem.* **1976**, *17*, 15−25.

(31) Yu, M. J.; Zhu, K. K.; Liu, Z. C.; Xiao, H. P.; Deng, W.; Zhou, X. G. *Appl. Catal., B* **2014**, *148*, 177−190.

(32) Xiao, H. P.; Liu, Z. C.; Zhou, X. G.; Zhu, K. K. *Catal. Commun.* **2013**, *34*, 11−15.

(33) Hara, M.; Waraksa, C. C.; Lean, J. T.; Lewis, B. A.; Mallouk, T. E. *J. Phys. Chem. A* **2000**, *104*, 5275−5280.

(34) Jiao, F.; Frei, H. *Angew. Chem., Int. Ed.* **2009**, *48*, 1841−1844.

(35) Lee, P. A.; Citrin, P. H.; Eisenberger, P.; Kincaid, B. M. *Rev. Mod. Phys.* **1981**, *53*, 769−806.

(36) Umena, Y.; Kawakami, K.; Shen, J. R.; Kamiya, N. *Nature* **2011**, *473*, 55−60.

(37) Kanan, M. W.; Yano, J.; Surendranath, Y.; Dinca, M.; Yachandra, V. K.; Nocera, D. G. *J. Am. Chem. Soc.* **2010**, *132*, 13692−13701.

(38) Risch, M.; Khare, V.; Zaharieva, I.; Gerencser, L.; Chernev, P.; Dau, H. *J. Am. Chem. Soc.* **2009**, *131*, 6936−3937.

(39) Zhang, M.; de Respinis, M.; Frei, H. *Nat. Chem.* **2014**, *6*, 362−367.

(40) Ahn, H. S.; Yano, J.; Tilley, T. D. *Energy Environ. Sci.* **2013**, *6*, 3080−3087.

(41) Zhu, K. K.; Hua, W. M.; Deng, W.; Richards, R. M. *Eur. J. Inorg. Chem.* **2012**, 2869−2876.

(42) Ravel, B.; Newville, M. *J. Synchrotron Radiat.* **2005**, *12*, 537−541.